



## Nanoparticle–membrane interactions

Claudia Contini, Matthew Schneemilch, Simon Gaisford & Nick Quirke

To cite this article: Claudia Contini, Matthew Schneemilch, Simon Gaisford & Nick Quirke (2017): Nanoparticle–membrane interactions, Journal of Experimental Nanoscience, DOI: [10.1080/17458080.2017.1413253](https://doi.org/10.1080/17458080.2017.1413253)

To link to this article: <https://doi.org/10.1080/17458080.2017.1413253>



© 2017 The Author(s). Published by Informa UK Limited, trading as Taylor & Francis Group.



Published online: 22 Dec 2017.



Submit your article to this journal [↗](#)



Article views: 118



View related articles [↗](#)



View Crossmark data [↗](#)

## Nanoparticle–membrane interactions

Claudia Contini<sup>a</sup>, Matthew Schneemilch<sup>a</sup>, Simon Gaisford<sup>b</sup> and Nick Quirke<sup>a</sup>

<sup>a</sup>Department of Chemistry, Imperial College London, London, United Kingdom; <sup>b</sup>Department of Pharmaceutics, UCL School of Pharmacy, University College London, London, United Kingdom

### ABSTRACT

Engineered nanomaterials have a wide range of applications and as a result, are increasingly present in the environment. While they offer new technological opportunities, there is also the potential for adverse impact, in particular through possible toxicity. In this review, we discuss the current state of the art in the experimental characterisation of nanoparticle–membrane interactions relevant to the prediction of toxicity arising from disruption of biological systems. One key point of discussion is the urgent need for more quantitative studies of nano–bio interactions in experimental models of lipid system that mimic *in vivo* membranes.

### ARTICLE HISTORY

Received 3 August 2017  
Accepted 29 November 2017

### KEYWORDS

nanotoxicity; nanomaterial;  
membrane interface;  
nanoparticle

## 1. Introduction

The rapid development of nanomaterials has led to an increase in the number and variety of engineered nanoparticles in the environment [1–4]. We are continuously exposed to products containing engineered nanomaterials (ENMs). Examples include batteries, catalysts, chemical coatings, packaging, electronic devices, biomedicines and cosmetics [5]. The expanding production of ENMs has led to serious concerns regarding their impact on human health and the environment in general (see for example the considerable investment made by the EU in nanosafety research in the H2020 programme, via the EU NanoSafety Cluster [6]). Nanoparticles (NPs) are easily dispersed in air and inhaled because of their nanoscale size [7,8]. Given their increasing use in sunscreens, cosmetics and other personal products they may enter the bloodstream by permeation through skin [1]. NPs are also found in pesticides, food products and packaging, and may enter the body via digestion [9,10]. Medical implants are another source of NPs in the human body being released by normal wear. NPs may also enter the body directly as nanomedicines or magnetic resonance imaging (MRI) contrast agents [11–14]. Given this degree of exposure, it is striking that implications for environmental and human health remain mostly unknown or poorly understood [15–17]. Identifying ENMs hazardous to natural organisms is difficult, given the wide variety of NPs, their diverse properties (eg particle material, size, shape, surface, charge, corona) and the complexity of biological entities (eg membrane and media composition, type of cell, cell cycle) [18]. The interaction of inorganic NPs with biological systems can lead to severe cytotoxic effects [17,19–24]. This

**CONTACT** Nick Quirke  n.quirke@imperial.ac.uk

cytotoxicity of ENMs is reported across a range of studies that highlight the biological impact of the NP exposure [5,25–28]. On the other hand, the cytotoxicity of NPs may also be used to enhance the antibacterial efficacy in light-activated antimicrobial surfaces [29]. Although there is a vast literature on nanoparticle–cell interactions [30–32], a detailed physicochemical description of adverse outcomes relevant to *in vivo* behaviour does not exist. In fact, most of the published studies offer no conclusive nano-toxicological data for *in vitro* models which might make it possible to predict an *in vivo* response. One of the main issues for *in vitro* experiments is the difficulty of recreating the exact environmental conditions that are present *in vivo*. Many of the end-points determined during *in vitro* testing have little or no relevance for the physiological and pathological changes in man or animals. In order to be able to distinguish between harmless and harmful nanomaterials significant progress must be made in understanding the relevant interactions or key initiating events at bio-nano interfaces and determining the NM properties relevant for these interactions.

One route to being able to predict nano-toxicological responses is through *in silico* approaches that, based on a detailed understanding of toxicity pathways and nano-bio molecular structure and dynamics, correlate materials descriptors (physical properties such as size, shape, electronic energy levels, lipid adsorption energies) with toxicological outcomes. Such a model is only possible if there exist reliable physical property data either from experiment or from nanoscale simulation [33–38]. Since one of the first steps in a toxicological response will be the nanoparticle meeting the cell membrane or lung fluid, it is clear that, prominent amongst the materials descriptors, will be the nanomaterial-bilayer interaction characterised by the free energy of adhesion per unit area of contact.

In this review, we discuss the current state of the art in the experimental characterisation of the nanoparticle-lipid membrane interaction, including structural and thermodynamic properties. We will also discuss NP uptake within membranes and the studies that visualise and quantify directly and indirectly, the NP-membrane interaction. One conclusion will be that there is an urgent need for quantitative studies of nano-bio interactions in experimental models of lipid systems that mimic *in vivo* membranes. Studies that could be used for the construction of an *in silico* model able to predict potential membrane perturbations and consequently, cytotoxic effects.

### **1.1. Nanoparticle–membrane interactions: elastic theory**

The cell is separated from the rest of the environment by a phospholipid bilayer barrier, the membrane. The cell membrane has the role of protecting the cell interior from the external environment allowing the maintenance of controlled conditions in the cell cytosol. The phospholipid bilayer contains proteins, cholesterol and lipopolysaccharides, located in the inner membrane or on its surface [39–41]. All these compounds allow the cell to respond to the external environment and to communicate with other cells. At the basis of this constant communication between cells and cell-environment, there is the solutes' transport across the membrane. Smaller and nonpolar molecules such as oxygen can pass across the membrane via simple Fickian diffusion. Larger and polar molecules (including ions), instead, need protein carrier mediated transport. In general large macromolecules are exchanged between the extracellular environment and the cell cytosol, *via* endocytosis (internalisation) and exocytosis (expulsion) [42,43]. These mechanisms are in

most cases controlled by the cell membrane *via* specific receptor-mediated interactions (eg clathrin, caveolin, flotillin mediated endocytosis) [42,44,45]. However, it has been demonstrated that NPs can also traverse the cell membrane *via* endocytosis (or exocytosis) without being involved in any specific receptor-mediated interaction [46–49]. Lipid membranes are highly flexible and the bilayer can be deformed due to NP adhesion on its surface leading to a full NP engulfment and its final uptake. This non-specific NP uptake has been also observed in vesicles suggesting that the NP uptake into membranes can be driven solely by general physicochemical interactions. Figure 1 shows three possible outcomes for NPs in contact with a cell membrane. If the adhesion energy is not sufficiently strong the nanoparticle will undergo Brownian collisions with the membrane but not adhere. Alternatively, the nanoparticle can sit at the membrane interface partially wrapped by the lipid bilayer. Finally, in the right conditions, the nanoparticle can be completely wrapped (engulfed) by the membrane and subsequently, detaches from the inner surface of the membrane, in a process known as fission, leaving a (typically) transient membrane pore [50].

Applying the model proposed by Helfrich [51,52], the passive NP engulfment process is governed by three energy contributions: adhesion energy in the contact area between NP and membrane,  $E_{adh}$ , membrane bending modulus,  $\kappa$  and membrane surface tension,  $\sigma$ . Adhesion energy drives the NPs into the membrane while the membrane's resistance to deformation, characterised by the bending and elastic moduli, oppose the engulfment process. Assuming a tensionless membrane and that the non-specific adhesion interaction is driving the process, NP engulfment occurs when the adhesion energy is sufficient to overcome the energy cost associated with bending the membrane around the particle surface. For this tensionless case, two parameters, adhesion energy and membrane bending modulus, define a critical radius,  $r_c$ , representing the minimum particle size for which the

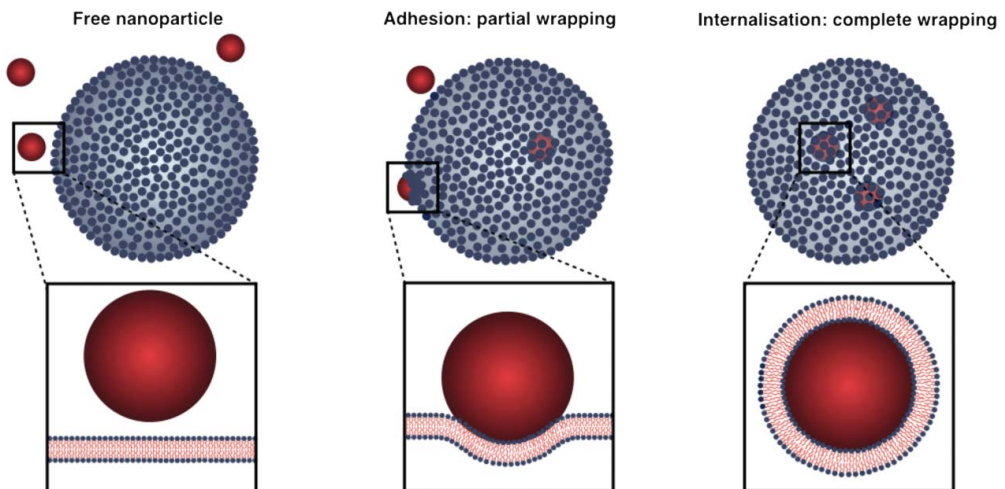


**Figure 1.** Three possible end points for NPs in contact with a membrane. Three possible outcomes for the NP-membrane interaction are illustrated: free NP in the environment, NP adhesion to membrane and NP complete wrapping and internalisation.

NP engulfment occurs [47,48,53,54]:

$$r_c^2 = \frac{2\kappa}{E_{\text{adh}}} \quad (1)$$

A NP with a radius equal or greater than the critical radius will undergo complete engulfment once contact has occurred. However, cells possess a membrane tension that ranges from 0.003 up to 0.4 mN·m<sup>-1</sup> depending on the cell state and type [55–57]. In presence of membrane tension, an additional energy cost is associated with the wrapping process and more work is required to pull the membrane towards the NP against the lateral membrane tension,  $\sigma$ . In this case, NPs larger than the critical radius will be partially wrapped, remaining in the membrane, the depth of penetration depending on the value of the surface tension. If we keep increasing the NP size beyond a second critical radius,  $r_{c,\sigma}$ , they will undergo a first order phase transition from partially wrapped to a fully wrapped (enveloped) state at  $r = r_{c,\sigma}$

$$r_{c,\sigma}^2 = \frac{2\kappa}{E_{\text{adh}} - \sigma}. \quad (2)$$

A characteristic length scale,  $\lambda$ , can be constructed based solely on the properties of the membrane [58]:

$$\lambda = \sqrt{\frac{2\kappa}{\sigma}}. \quad (3)$$

Deformations of the membrane on a scale less than  $\lambda$  are opposed primarily by bending energy, those larger than  $\lambda$  are predominantly opposed by tension energy. For example, for a cell membrane tension in the order of 0.05 mN·m<sup>-1</sup> and bending modulus values of 15  $k_B T$ , the length scale is approximately 50 nm [48]. Simulation [59] and experiment [60] suggest a bending modulus of  $\kappa \sim 23 k_B T$  ( $\sim 10^{-19}$  J) at 300 K for DPPC gives  $\sim 60$  nm. In what follows, we assume  $\kappa = 23 k_B T$  (unless otherwise stated) for the calculation of adhesion energy from the critical radius determined experimentally. The process is further complicated when multiple NPs are present. Successive engulfment events can drive up the tension as the membrane is consumed by the formation of a supported lipid bilayer on the engulfed NPs [61,62]. The tension will also increase when the NP size is comparable to the size of the cell or vesicle. In this case, the onset of adhesion will increase the cell's surface to volume ratio and therefore the membrane tension [58].

The key descriptors governing passive (non-specific) NP engulfment are thus: NP and cell size, NP-membrane adhesion energy, membrane elastic moduli and tension. Accurate nanoparticle size characterisation is therefore a key requirement [63–65]. There are also other important NP characteristics that can be experimentally controlled and which can influence the NP-membrane adhesion beside the size. Cationic NPs, for example, are often cytotoxic due to their attractive interaction with negatively charged membranes that leads to their rapid internalisation [66,67]. On the other hand, anionic NPs are generally less cytotoxic but they can easily undergo protein fouling when exposed to biological media. The rapid formation of a protein corona around the NP surface changes the NP

surface charge and size (also the tendency to particle agglomeration) which may influence the cellular uptake [62,68–70]. Another important factor influencing the rate of absorption and uptake is the NP shape. This is related to the increase of the surface area to volume ratio for cylindrical or rod shapes with a consequent increase of the surface available for absorption to the membrane [24,71]. Moreover, it has been recently observed that the details of the NP surface topology have considerable effect on cellular uptake [21]. The use of advanced microscopy techniques makes possible to visualise the surface topology of the most effective nanoscale vector present in nature, the virus and suggests that the presence of a pattern or domain on the NP surface facilitates cellular endocytosis by matching specific targets of the cellular surface. This new understanding is opening new horizons in the development of nanotechnology making it possible to manipulate, control and mimic membrane properties in order to create fully synthetic, nature inspired systems [72,73].

Understanding the mechanisms underlying the interaction between NPs and membranes is a complex task due to the numerous properties that characterise them. Figure 2 schematically illustrates these properties and the three dynamically interacting constituents: NP, surrounding microenvironment and membrane.

The following sections will focus on the experimental methods used to investigate the NP-membrane interaction.

## 1.2. 'Model' membranes

Model membranes are organised lipid structures that mimic the natural arrangement of lipids in cell membranes (see Figure 3).

These structures facilitate a systematic investigation of the changes of mechanical and thermodynamic properties of membranes when in contact with nanoparticles. They have many forms including supported or unsupported planar bilayer, spherical vesicles and interfacial monolayers [76–78] (Figure 3(A)). The simplified and shape-analogue lipid model membrane used to simulate a cell-like membrane structure is a spherical vesicle or liposome. Depending on size, unilamellar liposomes can be classified as small ('SUV', up to 100 nm in diameter), large ('LUV', with a diameter between 100 nm and 1  $\mu\text{m}$ ) and giant ('GUV', diameter larger than 1  $\mu\text{m}$ ). LUV and SUV are typically prepared via extrusion after hydration of a dry lipid film [79]. Preparing homogeneous and stable GUVs

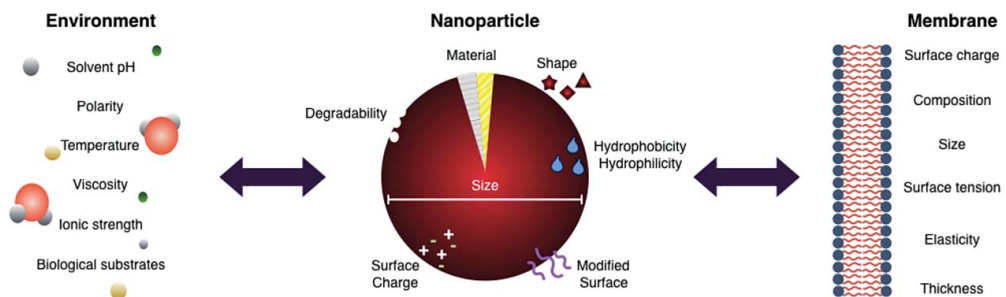


**Figure 2.** Properties that influence the NP-membrane interaction. The intrinsic characteristics of a NP, the surrounding environment and the biological substrate that influence the interaction between NPs and biological membranes.

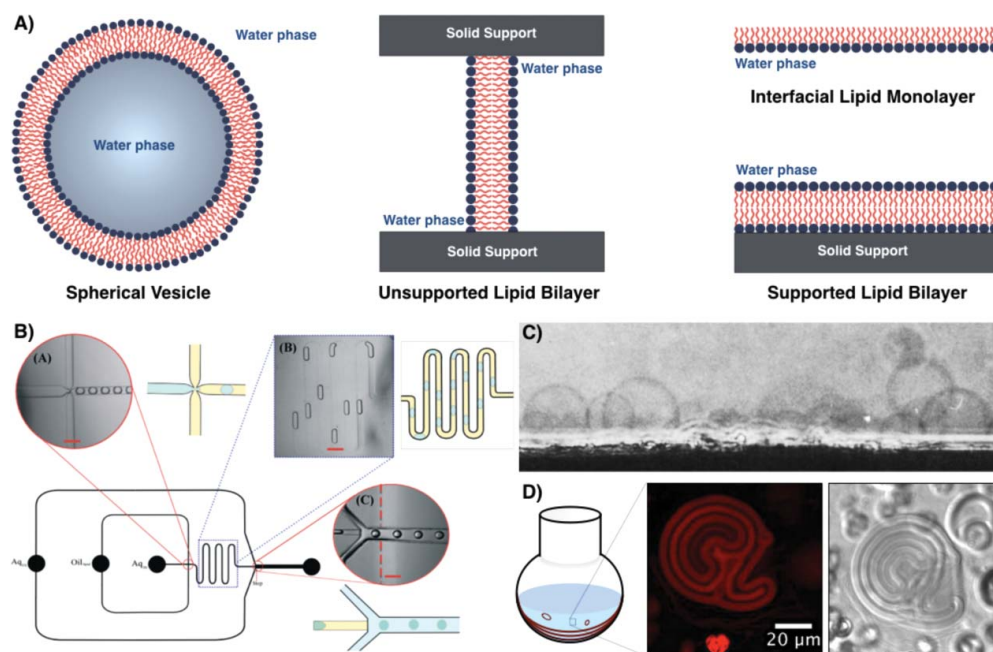


**Figure 3.** Schematic representation of model membrane structures and examples of lipid vesicle preparation techniques. Model membranes can be organised in different structures including spherical vesicles, unsupported and supported planar bilayers and interfacial monolayers (A). Giant unilamellar vesicles (GUVs) can be formed using microfluidic techniques (B) and via electroformation (C). Multilayer spherical membranes obtained by simply rehydrating a dry lipid film, confocal image, in fluorescence and bright field (D).

Source: Figure 3(B) is reprinted with permission from Karamdad et al. [74]. Figure 3(C) is reprinted with permission from Angelova et al. [75]. Published by The Royal Society of Chemistry. Copyright 1969 Royal Society of Chemistry.

can be more challenging. One route is to employ microfluidic methodologies an example of which is the innovative two-phase microfluidic platform shown in Figure 3(B) [74]. Others techniques widely used to create GUVs are gentle lipid film hydration and electroformation (Figure 3(C)) [75,80]. By simply rehydrating a dry lipid film with aqueous solvent, it is possible to create multilamellar vesicles with sizes ranging from nano to microscale (a fluorescence and bright field confocal image of giant multilamellar vesicle is shown in Figure 3(D)).

## 2. Measurement of NP-lipid bilayer interaction energies

In this section, we look at quantitative studies of nano-bio interactions in experimental models of lipid systems that mimic *in vivo* membranes.

### 2.1. Isothermal titration calorimetry (ITC)

ITC can be used to measure the heat of interaction (released or absorbed) between NPs and biomolecules, including lipids. This is a versatile technique able to directly measure the binding heat of interacting components freely dispersed in solution (no sample

immobilisation required) with no molecular weight limitation or requirement for molecular labelling. The two interacting components are initially separated: one solution is placed into the sample cell and the other is loaded in the injection syringe (titrant). On commencing the experiment, the titrant component is injected into the sample cell. As soon as the two components interact, they pass from free to a bound state and heat is consequently released or absorbed. These heat changes are recorded as the differential power applied to maintain a zero-temperature difference between the sample and reference cell (filled with the sample media). In a typical experiment (eg enzyme-substrate), the first injection usually represents 100% binding and results in a large deviation from the baseline, which decreases progressively with successive injections until the system is saturated and the deviation returns to the baseline range. Every heat peak/pulse generated by the multiple injections is then integrated and normalised for concentration. From this dependence, it is possible to obtain important binding parameters such as stoichiometry, affinity, enthalpy and entropy of interaction. The ITC instrument's sensitivity depends on the interacting compounds' affinity, concentration and instrument noise. For modern ITC instruments, the noise signal can be as little as 0.15–0.2 ncal.sec<sup>-1</sup> [81]. However, even if the modern ITC offers user-friendly settings such as control of injection time, number and titrant amount, measurements of small heats usually requires careful optimisation steps in order to minimise any heat effects associated with (i) mixing of mismatched solvents, (ii) dilution of the titrant and (iii) dilution of the ligand.

Together with standard enzyme-substrate and other substrate-ligand binding interactions, ITC has been used to investigate the interaction of NPs with diverse biological substrates. Lindman and co-workers used ITC to study the absorption of human serum albumin (HSA) to copolymeric NPs as a function of the NP hydrophobicity and surface curvature [82,83]. For this study, they made NPs with different degrees of hydrophobicity by changing the hydrophilic/hydrophobic monomer composition ratio within the copolymer. These NPs were created in a size range from 70 up to 700 nm. The ITC analysis was carried out by injecting firstly 1  $\mu\text{L}$  and subsequently 5  $\mu\text{L}$  of 40  $\mu\text{M}$  of HSA solution into the copolymeric NPs at a concentration of 1 mg.mL<sup>-1</sup> for a total of 60 injections. The ITC data showed an exothermic trend for all hydrophobicities. However, the system reached saturation at a lower number of injections for the more hydrophilic particles, indicating higher protein coverage for the more hydrophobic NPs. The authors also found that the NP surface curvature had an influence on the HSA binding. Higher curvature NPs (lower than 120 nm), presented a lower surface coverage than larger NPs. The authors' assumption is that larger NPs are comparable to a 'flat' surface at the protein interface. This allows absorbed proteins to interact with their neighbouring proteins stabilising and reinforcing the protein corona. The enthalpy changes calculated for the HSA titration into the different copolymeric nanoparticles varied from  $-104 \pm 53 \text{ kJ.mol}^{-1}$  for the more hydrophilic NP at 70 nm to  $-828 \pm 425 \text{ kJ.mol}^{-1}$  for the more hydrophobic NPs at 120 nm (note the very large uncertainties).

ITC has also been used to monitor biomolecule-inorganic NP interactions by Joshi and co-workers [84]. They investigated the interaction between amino acids (ie aspartic acid and lysine) and borohydride gold NPs (AuNPs). ITC measurements were performed injecting aliquots of 10  $\mu\text{L}$  of lysine (1 mM at pH 7 and 10 mM at pH 11) or aspartic acid (1 mM and 2 mM at pH 7) into  $\sim 1.5 \text{ mL}$  AuNP with an unknown concentration. This interaction between amino acids and AuNPs was exothermic and dependent on the pH in

the solution. This pH dependency was deduced by the lack or presence of ITC signals during the interaction at different solution pH, which indicated that the amino acids bind AuNPs only when their amine groups are in the unprotonated state. However, it is not clear which type of bond is involved in the AuNP-amino group interaction.

Loosli and co-workers used a similar approach to investigate and quantify the agglomeration process during the interaction between titanium dioxide NPs (TiNPs) and humic acid [85]. For the ITC study, the authors used 50 nm TiNPs and  $\sim 380$  nm humic acid. The titrations were performed using two orders of mixing: humic acid into TiNPs (type I) and vice versa (type II), schematically represented in Figure 4(A,B), respectively. Titrations were performed by injecting  $10 \mu\text{L}$  of titrant into the sample cell ( $\sim 1.5$  mL) for a total of 28 injections. Figure 4 shows the heat flows obtained by titrating  $0.1 \text{ g L}^{-1}$  TiNPs with  $250 \mu\text{M}$  humic acid (type I, A) and titrating  $37.5 \mu\text{M}$  humic acid with  $0.7 \text{ g L}^{-1}$  TiNPs (type II, B).

As shown in Figure 4, the ITC raw data show an exothermic trend (note the fluctuating baseline is not set to zero, heat flow less than the baseline signifies that an exothermic reaction is occurring) for both types of titration (type I and II) and led to enthalpy changes of  $-18.3$  and  $-11.7 \text{ kJ}\cdot\text{mol}^{-1}$ ; the free energy of the process was  $-37.9$  and  $-32.6 \text{ kJ}\cdot\text{mol}^{-1}$ , indicating the spontaneity of the reaction. This interaction depends on mixing order and concentration. In the type I titration, the humic acid is used at higher

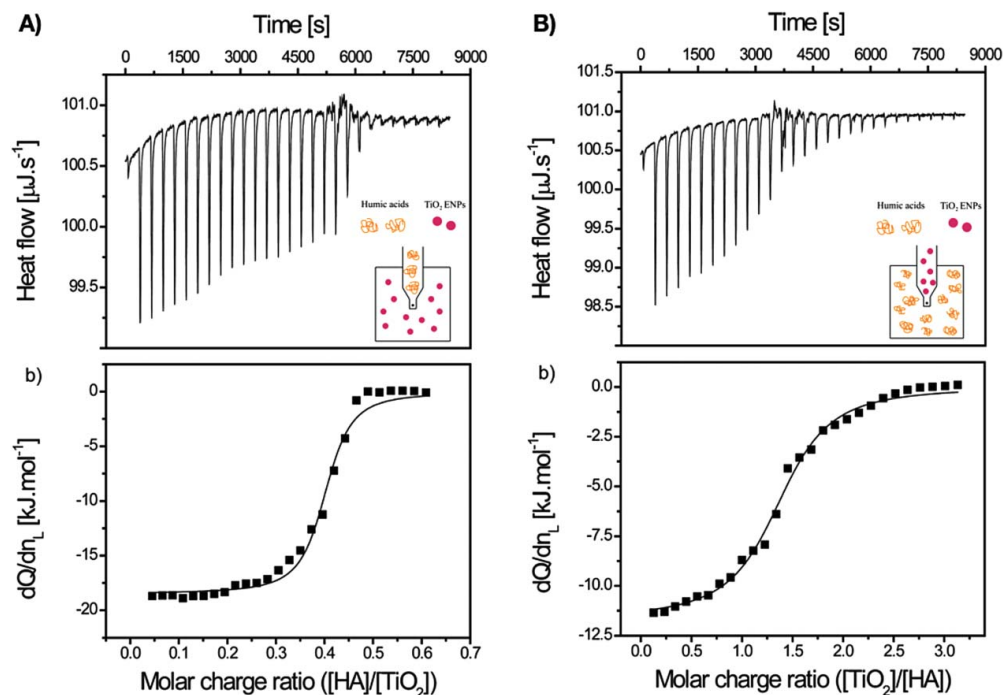


**Figure 4.** Heat flow and corresponding heat plot as a function of molar charge ratio for the two type of mixing titration: humic acid into TiNPs (A) and vice versa (B). The ITC data on the right shows the heat flow and corresponding heat plot of  $250 \mu\text{M}$  humic acid into  $0.1 \text{ g}\cdot\text{L}^{-1}$  TiNPs (A) and  $0.7 \text{ g}\cdot\text{L}^{-1}$  TiNPs into  $37.5 \mu\text{M}$  humic acid (B).

Source: Reprinted with permission from Loosli et al. [85]. Published by The Royal Society of Chemistry.

concentrations. The authors observed that by increasing the concentration of the interacting compounds, the enthalpy became more negative. This can be ascribed to the tendency of humic acid to self-agglomerate (which is concentration dependent) and to form larger agglomerates that bind more TiNPs.

We turn now to consider the interaction between lipid membranes and inorganic NP surfaces. Kettiger and co-workers [86] performed ITC measurements of NPs and SUVs. The authors used negatively and positively charged silica NPs (SNPs) 120 nm in diameter and around 30 nm POPC SUVs formed by extrusion and subsequent sonication. Dynamic light scattering showed that upon initial addition of SUVs to the anionic SNP solution, large lipid agglomerates were formed with a mean diameter of 1  $\mu\text{m}$ . Upon further addition of SUVs, a new population began to appear with a size around 0.1  $\mu\text{m}$  which was interpreted to represent isolated bilayer-coated SNPs. To confirm the agglomeration effect was caused by the negatively charged SNPs, the authors performed ITC measurements. Titrations were carried out by injecting 4  $\mu\text{L}$  aliquots of 3.8 and 7.6  $\text{mg}\cdot\text{mL}^{-1}$  SUV suspension into positively (1  $\text{mg}\cdot\text{mL}^{-1}$ ) and negatively (0.5  $\text{mg}\cdot\text{mL}^{-1}$ ) charged SNP solutions, respectively. Titration of positively charged SNPs did not show any signal of interaction. On the other hand, the negatively charged SNP titration showed measurable heat flux for the first three injections of SUVs only. This indicates that, under these experimental conditions, all the negatively charged SNPs present in the sample cell are completely bound to SUVs after a few injections. The enthalpy of adhesion per unit surface area was exothermic and constant over the temperature range between 15 and 40  $^{\circ}\text{C}$ . Given the detected enthalpy of adhesion of 0.04  $\text{cal}\cdot\text{g}^{-1}$ , and the authors' specific surface area of 35  $\text{m}^2\cdot\text{g}^{-1}$  for negatively charged SNP, we estimated an enthalpy of adhesion per unit surface of 4.8  $\text{mN}\cdot\text{m}^{-1}$ .

All these studies are clear examples of how ITC can be exploited as a powerful technique to probe the interaction between NPs and biomolecules and consequently, their potential nanotoxicity for organisms and the environment. In principle ITC allows us to determine all the thermodynamic parameters of interaction (eg enthalpy and entropy contribution, free energy, reaction stoichiometry and constant of affinity) in one experiment [87]. However, measuring the NP-biomolecule interaction can be challenging as it is often driven by unspecific binding, which leads to complex interaction trends (eg endothermic and exothermic contribution in the same heat flow or even single peak signals). For this reason, ITC has been primarily used as a qualitative method to probe the differences in the type of interaction or presence/absence of interaction. Clearly before it can become a routine technique for quantifying nanomaterial heats of adhesion, both experimental protocols and the interpretation of the heat flows needs to be considerably improved, perhaps with the assistance of molecular methods such as molecular simulation and theory.

## 2.2. Other methods

Another direct method of measuring the adhesion energy between inorganic surfaces and lipid bilayers is via the surface force apparatus [88], as utilised by Anderson and co-workers [89]. In their study, DMPC SLB formed by Langmuir–Blodgett deposition or vesicle fusion were interrogated with amorphous silica surfaces made by electron deposition. Both the silica and bilayer were formed on two mica cylinders approximately 2 cm in radius. The cylinders were placed in a 90 $^{\circ}$  crossed position with the bottom cylinder

parallel to the observer's point of view in Figure 5. The normal force profiles in Figure 5 display an initial repulsion at distances less than 10 nm before the surface and bilayer jump into contact. The silica surface was then withdrawn and jumps out of contact when the applied force exceeds the force of adhesion.

The adhesion energy per unit area, estimated from the maximum attractive force within the Derjaguin approximation [90], was 0.5 and 1  $\text{mN}\cdot\text{m}^{-1}$  for the vesicle fusion and Langmuir–Blodgett deposition SLB, respectively.

Direct measurements of the adhesion energy of DMPC lipid bilayers on gold electrodes have been performed in the Lipkowski laboratory [91]. The method relies on the observation that SLBs change their morphology when a potential difference is applied between the supporting electrode and another electrode in the aqueous medium. The bilayer structures, inferred from neutron reflectivity profiles obtained *in situ*, are represented schematically in Figure 6 at selected potential differences and surface density charge.

The neutron reflectivity profiles of the bilayer suggested that increasing the Au electrode charge density results in an increase in the bilayer thickness (membrane swelling) due to increasing water content inside the bilayer region. It is important to notice that at a relatively high electrode potential (eg  $\sim -0.9$  V for the 7:3 DMPC/cholesterol mixture shown in Figure 6) the surface charge curve of the bilayer-covered electrode (ie red and point-dotted curve in figure) equals the pure electrode profile (ie black and squared-dotted curve in figure) meaning that the bilayer reversibly desorbs from the surface. By monitoring the current associated with stepping the potential, it was possible to calculate the surface charge density. In this way, the authors constructed surface charge vs. electrode potential curves in both the absence and presence of a bilayer. Integrating the difference between these two curves gives the adhesion energy per unit area. For a pure DMPC bilayer this was found to be 40  $\text{mN}\cdot\text{m}^{-1}$ . Unfortunately, this method is inapplicable to insulating materials such as silica.

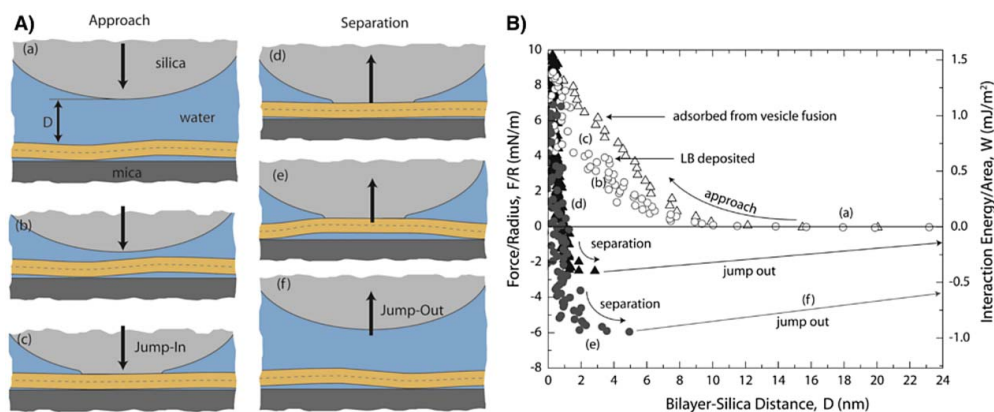


**Figure 5.** Schematic representation of the surfaces (A) and force-distance profiles (B) during interaction between the silica surface and the lipid bilayer on a mica support. The schematic representation (A) illustrates the distinct stages identified during the silica surface-membrane interaction: approach to membrane (a), initial repulsion (b), jump-in to adhesive contact (c), surface-membrane separation (d and e), jump-out with the two surfaces separating apart. The force-distance and adhesion energy profiles are shown on the right (B) for bilayers formed by Langmuir–Blodgett deposition (circles) and vesicle fusion (triangles). Reprinted with permission from Anderson et al. [89]. Copyright 2009 American Chemical Society.

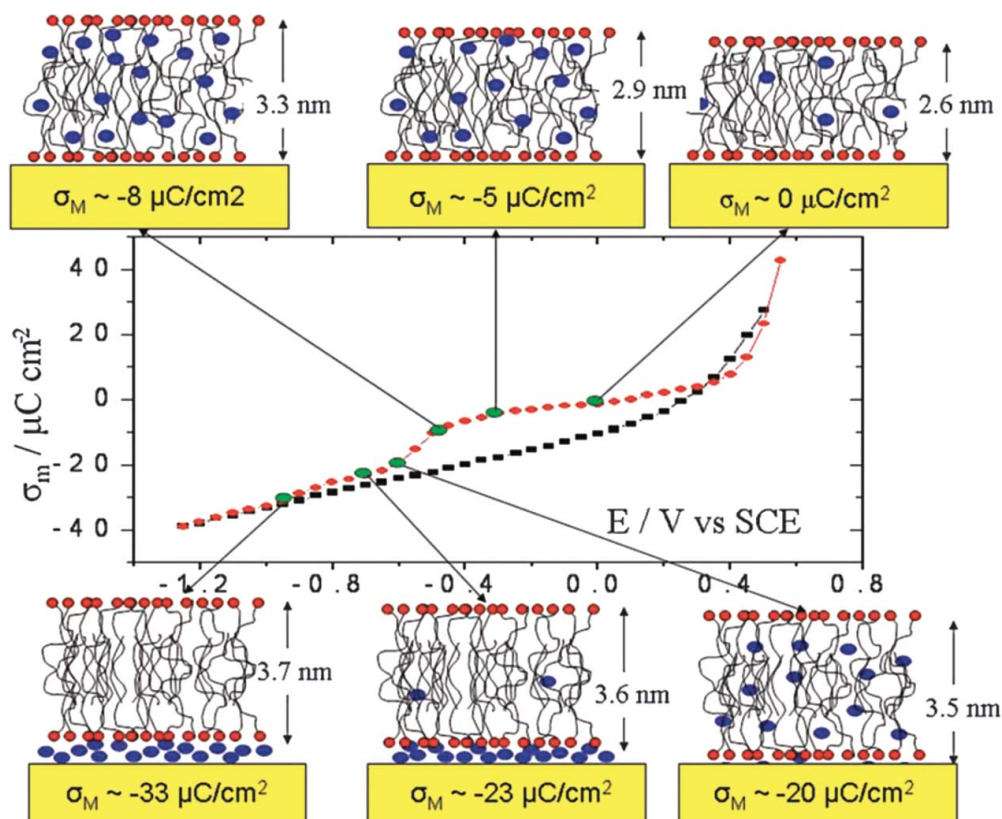


**Figure 6.** Applied electrode potential vs. surface density charge and representations of the corresponding bilayer structures. The surface charge density on the supporting Au electrode is plotted against the applied potential in the absence (black, square-dotted line) and presence (red, point-dotted line) of a supported lipid bilayer on the electrode. The bilayer was formed by 7:3 DMPC/cholesterol vesicle fusion. The membrane structure and thickness are schematically represented at selected potentials. Source: Reprinted with permission from Lipkowski [92]. Copyright 2010 from Royal Society of Chemistry.

A similar investigation on the effect of electric field on DOPC lipid layers (mono and bilayer) was carried out by Vakurov and co-workers [93]. For the experiments, they performed direct AFM measurements of the lipid layers deposited on a wafer-based Hg film electrode. These AFM measurements allowed the measurement of the lipid layer thickness and resistance to AFM penetration as a function of the applied potential. The authors observed the same  $\sim 1$  nm increase of the bilayer thickness reported by the Lipokowski group [91], at around 1.02 V due to the increase of water content in the interface between bilayer and surface. However, at higher potentials (more than  $-1.35$  V), the DOPC bilayer thickness drastically decreases, compacting on the Hg surface.

### 3. Observing the NP-lipid bilayer interaction

In recent decades, imaging techniques have been developed to directly visualise the NP-membrane interaction at the micro and nanoscale and its effect on the membrane integrity. In particular transmission, scanning and cryogenic transmission electron

microscopies (TEM, SEM and Cryo-TEM), atomic force microscopy (AFM) and fluorescence microscopy are in routine use [94–97]. Depending on the NP material, size and charge, these techniques allow us to directly investigate different mechanisms of interaction (eg absorption or permeation) by locating the NP position with respect to the membrane and to directly observe the consequences for the membrane, such as changes in permeability or its complete disruption [98]. In particular, cryo-TEM allows for the investigation of the interaction of NPs with suspended spherical lipid vesicles and any bilayer elastic perturbation.

Le Bihan and co-workers [99] captured cryo-TEM images of LUVs composed of DOPC lipids after incubation with SNPs. SNPs were created using 7 nm diameter maghemite nanocrystals as seeds for growth process in order to improve the NPs' contrast in the TEM images. LUVs (ie 200 nm in diameter) were prepared by extrusion. Their work provides compelling evidence that the particles do indeed translocate the membranes via the engulfment mechanism (membrane wrapping and internalisation). The authors show clear images of internalised SNPs exhibiting a SLB on their surfaces. Additionally, they show that SNPs are able to translocate the outer bilayer of double-layered vesicles but not the inner bilayer since the SLB generated during the initial engulfment prevents close contact between the particle and the inner bilayer, in effect decreasing the adhesion energy. Of all the SNPs exposed to the vesicles, with diameters ranging from 15 to 190 nm, only particles greater than 20 nm were completely engulfed while 15–20 nm particles adhered to the surface. Clearly, this implies that the critical radius for their particular SNPs is less than 15 nm, which in turn, using Equation (1) and  $\kappa = 10^{-19}$  J, sets a lower limit on the adhesion energy per unit area of approximately  $0.8 \text{ mN}\cdot\text{m}^{-1}$ .

Michel et al. studied similar solutions containing unilamellar DOPC vesicles and SNPs, where the vesicles had a hydrodynamic radius of 58 nm and the SNPs were 16 nm in diameter [100]. By using SNPs close in size to the critical radius they attempted to slow down the rate of the engulfment process and thereby study the dynamics. They monitored the system using dynamic light scattering and cryo-TEM (micrographs shown in Figure 7). Initially, a few SNPs underwent complete engulfment, increasing the vesicle tension as the

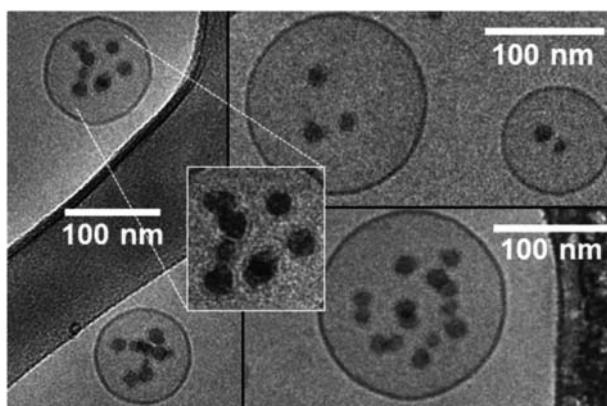


**Figure 7.** Cryo-TEM images of SNPs internalised within a vesicle. The Cryo-TEM images and magnified detail show the presence of a full lipid bilayer coverage on the SNP surface as a result of the engulfment process.

Source: Reprinted with permissions from Michel et al. [100]. Copyright 2014 from John Wiley and Sons.

membrane was consumed during SLB formation. The remaining SNPs adhered to the vesicles but they were not engulfed due to the consequent tension increase. SUV fusion, occurring on much longer timescales, led to the formation of larger vesicles with lower tension thereby allowing the remaining SNPs to become fully engulfed. Increasing the SNP concentration further slowed down the fusion process due to the mutual repulsion of adsorbed SNPs.

In another study involving SNPs, Roiter and co-workers [101] utilised a geometry which isolated the balance between adhesion and bending energies without the complicating factor of membrane tension. SNPs with diameters ranging from 1 to 140 nm were positioned on a mica wafer and then a DMPC bilayer was deposited by adsorption from solution. The 3D images shown in Figure 8 were constructed from AFM measurements conducted on the same areas before and after bilayer deposition.

Only NPs with a diameter less than 1.2 nm and greater than 22 nm were fully covered by an adsorbed lipid bilayer following the contours of the surface. On the other hand, a bilayer formed pores around SNPs with diameters in the range from 1.2 to 22 nm. The formation of pores around NPs sized between 1.2 and 5 nm was barely detectable by AFM due to the similarity between the bilayer thickness ( $\sim 5$  nm) and the NP diameter (3.4 nm in Figure 8(B)). To confirm the presence of pores, insulin was added, which absorbs on the exposed NPs surface where it is readily detected by AFM. The critical radius of 11 nm identified in this study suggests an adhesion energy per unit area of approximately  $1.5 \text{ mN}\cdot\text{m}^{-1}$  (Equation (1),  $\kappa = 10^{-19} \text{ J}$ ).

Zhang and co-workers studied the effect of concentrated ( $500 \mu\text{g mL}^{-1}$ ) SNP solutions on DOPC GUVs ( $4\text{--}20 \mu\text{m}$  in diameter) prepared via electroformation [102]. Confocal microscopy images of vesicles after exposure to 18 nm diameter SNPs show the presence of microscale pores as shown in the left panel of Figure 9.

These pores are indicative of large membrane tension, the high density of SNPs adhering to the surface appears to stabilise the vesicles. Large SNPs of 182 nm diameter, on the other hand, are unable to prevent eventual vesicle rupture. The images are complemented by calculations of lipid diffusion coefficients based on the mobility of fluorescent probes within the vesicle membranes. Upon exposure to 18 nm SNPs the diffusion coefficient decreased from  $3.1 \pm 0.34$  to  $0.25 \pm 0.14 \mu\text{m}^2 \text{ s}^{-1}$ , whereas the 182 nm particles increased

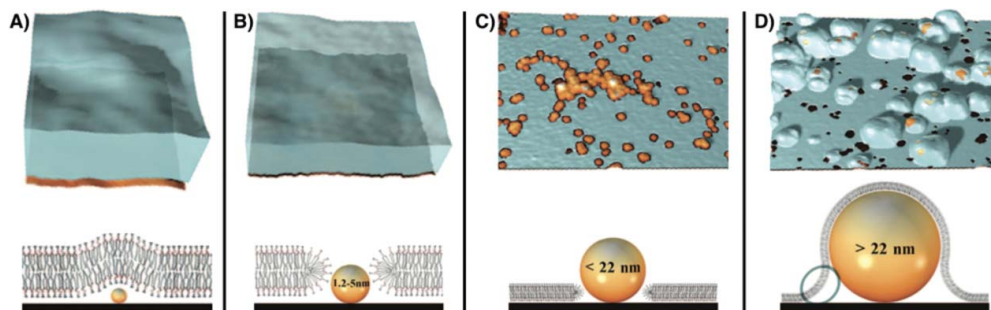


**Figure 8.** 3D representation of AFM measurement and correspondent schematics of the lipid bilayer deposition on SNPs with different size. Schematics of lipid bilayer formation on silica NPs with diameter smaller than 1.2 (A), between 1.2 and 5 nm (B), up to 22 nm (C) and larger than 22 nm (D) with corresponding AFM 3D reconstructions.

Source: Figures adapted with permission from Roiter et al. [101]. Copyright 2008 from American Chemical Society.

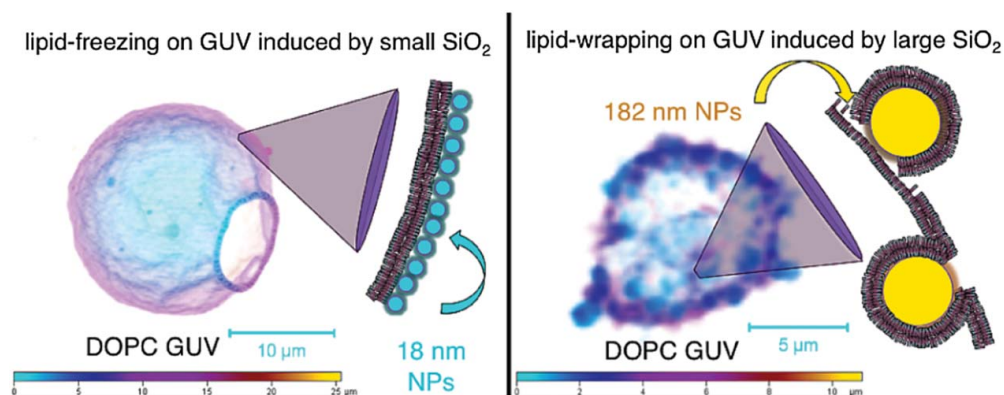


**Figure 9.** Images of vesicles in concentrated SNP solutions. Confocal laser scanning microscopy images of GUVs and their schematic representation during the interaction with two populations of SNPs (18 and 182 nm, on the left and right, respectively).

Source: Reprinted with permission from Zhang et al. [102]. Copyright 2012 from American Chemical Society.

the diffusion coefficient to  $7.14 \pm 2.4 \mu\text{m}^2 \text{s}^{-1}$ . The origin of these different effects is unclear. Interestingly, the authors postulate that the smaller SNPs stabilise the pores by acting as a line-agent reducing the line tension around the pore perimeter.

Strobl and co-workers [103] examined the effect of thermodynamic membrane state (ie fluid and gel state) on uptake by exposing 123 nm and 42 nm SNPs to DMPC GUVs at temperatures above and below the lipids' phase transition temperature. In Figure 10, images captured by fluorescence microscopy show vesicles in fluid and gel state after incubation with the two populations of SNPs.

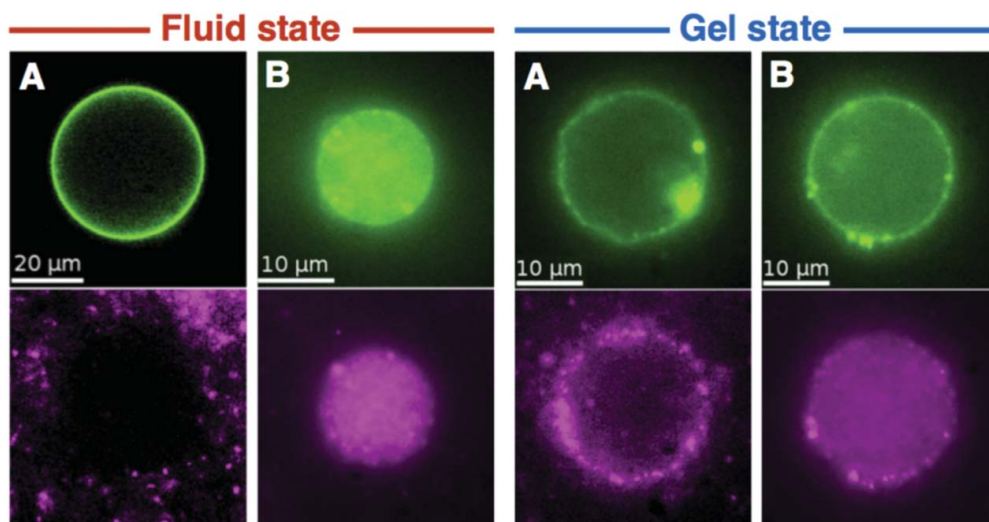


**Figure 10.** Fluorescence microscopy images of fluorescent GUV (green, top row) in fluid and gel state, interacting with SNPs (magenta, bottom row). Fluid state (left): (A) After 30 min incubation with 123 nm diameter particles, (B) after 10 min exposure to 42 nm diameter particles. Gel state (right): (A) After 15 min exposure to 123 nm diameter particles, (B) after 10 min exposure to 42 nm diameter particles.

Source: Adapted with permission from Strobl et al. [103]. Copyright 2014 from Beilstein-Institut.

In Figure 10, the lipids appear green (top panel) while the particles appear magenta (bottom panel). When the vesicles were in their fluid state, only 42 nm SNPs were engulfed while 123 nm SNPs remained suspended in the surroundings showing no signs of adhesion. On the other hand, when the GUVs were in the gel state, adhesion and engulfment were strongly observed for both SNP size populations, although the number of smaller SNPs engulfed seems significantly less than when the vesicles were in the fluid state. The last observation could be understood in terms of the increase in membrane rigidity associated with the gel phase (roughly an order of magnitude greater than in the fluid phase) which can be expected to increase the critical radius from 11 to approximately 35 nm, preventing SNPs in the lower range of the size distribution from adhering. The authors ascribe the relatively low incidence of engulfment for the larger particles to membrane tension increases associated with membrane consumption for SLB formation. According to elastic theory up to 9 times as many smaller particles should become engulfed before tension blocks further internalisation events. This does not explain why the large particles did not adhere to the fluid phase vesicles.

#### 4. Conclusions

The experiments described in the preceding sections illustrate the progress made in characterising NP-membrane interactions but also demonstrate the paucity of data. Most experiments are for SNPs in contact with single component membranes for which adsorption energies are very small,  $\sim 1 \text{ mN}\cdot\text{m}^{-1}$ . The only non-silica data are for gold, where the adsorption energy per unit area is much larger at  $40 \text{ mN}\cdot\text{m}^{-1}$ . This last value has been used to demonstrate the vital importance of accurate experimental data for calibrating classical interaction potentials. In a molecular dynamics simulation of DMPC membranes on gold the use of semi-empirical cross terms to estimate interaction potentials resulted in a discrepancy in the adhesion energy of 25% compared to experiment [34]. For the experimental adhesion energy on silica, the situation is further complicated by the role that the atomic structure (for example the silanol density and the degree of ionisation) plays in determining the adhesion energy. Molecular simulations show that there is a factor of 4 difference between the adhesion energy of lipid bilayers on a cristobalite surface and that on an amorphous surface with silanol bonds [104].

Given the large number of different types of engineered nanoparticles of relevance to toxicological studies, the fact that their properties will vary depending on the environmental conditions and the lack of experimental data on basic properties such as membrane adhesion energy, it is clear that we face significant obstacles to progress in developing predictive toxicological models. Reliable data for well-characterised materials are urgently required both for mechanistic molecular simulation studies of key initiating events in toxicological response as well as for structure/property correlations designed to predict toxicological end points. Indirect methods based on estimating adhesion energy from the critical radii for membrane engulfment rely on a knowledge of membrane properties which we may not have. The combination of modern microscopy with direct measurements of heat flows as in ITC is a promising way forward that could *in principle* provide the required data on the interactions of nanomaterials with both model and actual cell membranes.

## Acknowledgement

We would like to acknowledge the European Union's Horizon 2020 research and innovation programme for funding support.

## Disclosure statement

No potential conflict of interest was reported by the authors.

## Funding

We acknowledge financial support through the European Union's Horizon 2020 research and innovation programme (Smartnanotox project under grant agreement No. 686098).

## References

- [1] Gottschalk F, Nowack B. The release of engineered nanomaterials to the environment. *J Environ Monit.* 2011;13(5):1145–1155.
- [2] Garner KL, Keller AA. Emerging patterns for engineered nanomaterials in the environment: a review of fate and toxicity studies. *J Nanoparticle Res.* 2014;16(8):2503.
- [3] Colvin VL. The potential environmental impact of engineered nanomaterials. *Nat Biotechnol.* 2003;21(10):1166–1170.
- [4] Malysheva A, Lombi E, Voelcker NH. Bridging the divide between human and environmental nanotoxicology. *Nat Nanotechnol.* 2015;10(10):835–844.
- [5] Nel A, Xia T, Mädler L, et al. Toxic potential of materials at the nanolevel. *Science.* 2006;311(5761):622–627.
- [6] EU NanoSafety cluster – about the NanoSafety cluster. Available from: <https://www.nanosafetycluster.eu/>.
- [7] Shaffer RE, Rengasamy S. Respiratory protection against airborne nanoparticles: a review. *J Nanoparticle Res.* 2009;11(7):1661.
- [8] Bakand S, Hayes A, Dechsakulthorn F. Nanoparticles: a review of particle toxicology following inhalation exposure. *Inhalation Toxicol.* 2012;24(2):125–135.
- [9] Souza VGL, Fernando AL. Nanoparticles in food packaging: biodegradability and potential migration to food – a review. *Food Packag Shelf Life.* 2016;8:63–70.
- [10] He X, Hwang H-M. Nanotechnology in food science: functionality, applicability, and safety assessment. *J Food Drug Anal.* 2016;24(4):671–681.
- [11] Cristina B, Ivan IP, Kevin R. Nanomaterials and nanoparticles: sources and toxicity. *Biointerphases.* 2007;2(4):MR17–MR71.
- [12] Kendall M, Lynch I. Long-term monitoring for nanomedicine implants and drugs. *Nat Nanotechnol.* 2016;11(3):206–210.
- [13] Scharf B, Clement CC, Zolla V, et al. Molecular analysis of chromium and cobalt-related toxicity. *Sci Rep.* 2014;4:5729.
- [14] De Jong WH, Borm PJ. Drug delivery and nanoparticles: applications and hazards. *Int J Nanomed.* 2008;3(2):133–149.
- [15] Lohse S. Nano contaminants: how nanoparticles get into the environment. Sustainable Nano 2014, May 13. Available from: <https://sustainable-nano.com/2014/05/13/nano-contaminants-how-nanoparticles-get-into-the-environment/>
- [16] Nowack B, Bucheli TD. Occurrence, behavior and effects of nanoparticles in the environment. *Environ Pollut.* 2007;150(1):5–22.
- [17] Sajid M, Ilyas M, Basheer C, et al. Impact of nanoparticles on human and environment: review of toxicity factors, exposures, control strategies, and future prospects. *Environ Sci Pollut Res.* 2015;22(6):4122–4143.

- [18] Nel AE, Mädler L, Velegol D, et al. Understanding biophysicochemical interactions at the nano–bio interface. *Nat Mater.* 2009;8(7):543–557.
- [19] Joris F, Manshian BB, Peynshaert K, et al. Assessing nanoparticle toxicity in cell-based assays: influence of cell culture parameters and optimized models for bridging the in vitro–in vivo gap. *Chem Soc Rev.* 2013;42(21):8339–8359.
- [20] Lewinski N, Colvin V, Drezek R. Cytotoxicity of nanoparticles. *Small.* 2008;4(1):26–49.
- [21] Verma A, Stellacci F. Effect of surface properties on nanoparticle–cell interactions. *Small.* 2010;6(1):12–21.
- [22] Yildirim L, Thanh NTK, Loizidou M, et al. Toxicology and clinical potential of nanoparticles. *Nano Today.* 2011;6(6):585–607.
- [23] Yamashita K, Yoshioka Y, Higashisaka K, et al. Silica and titanium dioxide nanoparticles cause pregnancy complications in mice. *Nat Nanotechnol.* 2011;6(5):321–328.
- [24] Mu Q, Jiang G, Chen L, et al. Chemical basis of interactions between engineered nanoparticles and biological systems. *Chem Rev.* 2014;114(15):7740–7781.
- [25] Donaldson K, Stone V, Tran C, et al. Nanotoxicology. *Occup Environ Med.* 2004;61(9):727–728.
- [26] Oberdörster G, Oberdörster E, Oberdörster J. Nanotoxicology: an emerging discipline evolving from studies of ultrafine particles. *Environ Health Perspect.* 2005;113(7):823–839.
- [27] Shvedova AA, Kisin ER, Mercer R, et al. Unusual inflammatory and fibrogenic pulmonary responses to single-walled carbon nanotubes in mice. *Am J Physiol – Lung Cell Mol Physiol.* 2005;289(5):L698–L708.
- [28] Pietroiusti A. Health implications of engineered nanomaterials. *Nanoscale.* 2012;4(4):1231–1247.
- [29] Macdonald TJ, Wu K, Sehmi SK, et al. Thiol-capped gold nanoparticles swell-encapsulated into polyurethane as powerful antibacterial surfaces under dark and light conditions. *Sci Rep.* 2016;6:39272.
- [30] Shang L, Nienhaus K, Nienhaus GU. Engineered nanoparticles interacting with cells: size matters. *J Nanobiotechnol.* 2014;12:5.
- [31] Cheng L-C, Jiang X, Wang J, et al. Nano–bio effects: interaction of nanomaterials with cells. *Nanoscale.* 2013;5(9):3547–3569.
- [32] Mailänder V, Landfester K. Interaction of nanoparticles with cells. *Biomacromolecules.* 2009;10(9):2379–2400.
- [33] Lai K, Wang B, Zhang Y, et al. Computer simulation study of nanoparticle interaction with a lipid membrane under mechanical stress. *Phys Chem Chem Phys.* 2012;15(1):270–278.
- [34] Schneemilch M, Quirke N. Free energy of adsorption of supported lipid bilayers from molecular dynamics simulation. *Chem Phys Lett.* 2016;664:199–204.
- [35] Ding H, Ma Y. Interactions between Janus particles and membranes. *Nanoscale.* 2012;4(4):1116–1122.
- [36] Lopez H, Brandt EG, Mirzoev A, et al. Multiscale modelling of bionano interface. Modelling the toxicity of nanoparticles 2017 (Advances in Experimental Medicine and Biology). Cham, ZG: Springer. p. 173–206 . Available from: [https://link.springer.com/chapter/10.1007/978-3-319-47754-1\\_7](https://link.springer.com/chapter/10.1007/978-3-319-47754-1_7)
- [37] M. Meunier. Industrial applications of molecular simulations. Boca Raton, USA: CRC Press; 2011.
- [38] Quirke NKEG. Molecular simulation and industrial applications: methods, examples, and prospects. Amsterdam, The Netherlands: Gordon and Breach Science Publishers. (Current topics in molecular simulation, v. 1.), 1996.
- [39] Cooper GM, Sunderland, MA: Sinauer Associates. Cell membranes. 2000 Available from: <https://www.ncbi.nlm.nih.gov/books/NBK9928/>
- [40] Chapman D. Phospholipid bilayers physical principles and models. *Cell Biochem Funct.* 1988;6(2):147–148.
- [41] van Meer G, Voelker DR, Feigenson GW. Membrane lipids: where they are and how they behave. *Nat Rev Mol Cell Biol.* 2008;9(2):112–124.

- [42] Kumari S, Mg S, Mayor S. Endocytosis unplugged: multiple ways to enter the cell. *Cell Res.* **2010**;20(3):256–275.
- [43] Conner SD, Schmid SL. Regulated portals of entry into the cell. *Nature.* **2003**;422(6927):37–44.
- [44] McMahon HT, Boucrot E. Molecular mechanism and physiological functions of clathrin-mediated endocytosis. *Nat Rev Mol Cell Biol.* **2011**;12(8):517–533.
- [45] Doherty GJ, McMahon HT. Mechanisms of endocytosis. *Annu Rev Biochem.* **2009**;78:857–902.
- [46] Kettler K, Veltman K, van de Meent D, et al. Cellular uptake of nanoparticles as determined by particle properties, experimental conditions, and cell type. *Environ Toxicol Chem.* **2014**;33(3):481–492.
- [47] Lipowsky R, Döbereiner H-G. Vesicles in contact with nanoparticles and colloids. *EPL Europhys Lett.* **1998**;43:219–225.
- [48] Zhang S, Gao H, Bao G. Physical principles of nanoparticle cellular endocytosis. *ACS Nano.* **2015**;9(9):8655–8671.
- [49] Lin J, Zhang H, Chen Z, et al. Penetration of lipid membranes by gold nanoparticles: insights into cellular uptake, cytotoxicity, and their relationship. *ACS Nano.* **2010**;4(9):5421–5429.
- [50] Campelo F, Malhotra V. Membrane fission: the biogenesis of transport carriers. *Annu Rev Biochem.* **2012**;81(1):407–427.
- [51] Helfrich W. Elastic properties of lipid bilayers: theory and possible experiments. *Z Nat.forsch. Teil C Biochem Biophys Biol Virol.* **1973**;28(11):693–703.
- [52] Deserno M. Elastic deformation of a fluid membrane upon colloid binding. *Phys Rev E.* **2004**;69(3):031903.
- [53] Zhang S, Li J, Lykotrafitis G, et al. Size-dependent endocytosis of nanoparticles. *Adv Mater.* **2009**;21:419–424.
- [54] Agudo-Canalejo J, Lipowsky R. Uniform and Janus-like nanoparticles in contact with vesicles: energy landscapes and curvature-induced forces. *Soft Matter.* **2017 Feb 10** 13:2155–2173.
- [55] Morris CE, Homann U. Cell surface area regulation and membrane tension. *J Membr Biol.* **2001**;179(2):79–102.
- [56] Schweitzer Y, Lieber AD, Keren K, et al. Theoretical analysis of membrane tension in moving cells. *Biophys J.* **2014**;106(1):84–92.
- [57] Raucher D, Sheetz MP. Membrane expansion increases endocytosis rate during mitosis. *J Cell Biol.* **1999**;144(3):497–506.
- [58] Deserno M, Gelbart WM. Adhesion and wrapping in colloid–vesicle complexes. *J Phys Chem B.* **2002**;106(21):5543–5552.
- [59] Tarazona P, Chacón E, Bresme F. Thermal fluctuations and bending rigidity of bilayer membranes. *J Chem Phys.* **2013**;139(9):94902.
- [60] Nagle JF. Introductory lecture: basic quantities in model biomembranes. *Faraday Discuss.* **2013**;161:11–150.
- [61] Messerschmidt C, Hofmann D, Kroeger A, et al. On the pathway of cellular uptake: new insight into the interaction between the cell membrane and very small nanoparticles. *Beilstein J Nanotechnol.* **2016**;7:1296–1311.
- [62] Lesniak A, Salvati A, Santos-Martinez MJ, et al. Nanoparticle adhesion to the cell membrane and its effect on nanoparticle uptake efficiency. *J Am Chem Soc.* **2013**;135(4):1438–1444.
- [63] Robertson JD, Rizzello L, Avila-Olias M, et al. Purification of nanoparticles by size and shape. *Sci Rep* **2016 Jun 8**;6:27494.
- [64] Cho EJ, Holback H, Liu KC, et al. Nanoparticle characterization: state of the art, challenges, and emerging technologies. *Mol Pharm.* **2013**;10(6):2093–2110.
- [65] Montes-Burgos I, Walczyk D, Hole P, et al. Characterisation of nanoparticle size and state prior to nanotoxicological studies. *J Nanoparticle Res.* **2010**;12(1):47–53.
- [66] Fröhlich E. The role of surface charge in cellular uptake and cytotoxicity of medical nanoparticles. *Int J Nanomedicine.* **2012**;7:5577–5591.

- [67] Leroueil PR, Berry SA, Duthie K, et al. Wide varieties of cationic nanoparticles induce defects in supported lipid bilayers. *Nano Lett.* 2008;8(2):420–424.
- [68] Mahmoudi M, Lynch I, Eftehadi MR, et al. Protein–nanoparticle interactions: opportunities and challenges. *Chem Rev.* 2011;111(9):5610–5637.
- [69] Monopoli MP, Walczyk D, Campbell A, et al. Physical–chemical aspects of protein corona: relevance to in vitro and in vivo biological impacts of nanoparticles. *J Am Chem Soc.* 2011;133(8):2525–2534.
- [70] Weissleder R, Kelly K, Sun EY, et al. Cell-specific targeting of nanoparticles by multivalent attachment of small molecules. *Nat Biotechnol.* 2005;23(11):1418–1423.
- [71] Salatin S, Maleki Dizaj S, Yari Khosroushahi A. Effect of the surface modification, size, and shape on cellular uptake of nanoparticles. *Cell Biol Int.* 2015;39(8):881–890.
- [72] Fernandez-Trillo F, Grover LM, Stephenson-Brown A, et al. Vesicles in nature and the laboratory: elucidation of their biological properties and synthesis of increasingly complex synthetic vesicles. *Angew Chem Int Ed.* 2017;56(12):3142–3160.
- [73] Joseph A, Contini C, Cecchin D, et al. Chemotactic synthetic vesicles: design and applications in blood-brain barrier crossing. *Sci Adv.* 2017;3(8):e1700362.
- [74] Karamdad K, Law RV, Seddon JM, et al. Preparation and mechanical characterisation of giant unilamellar vesicles by a microfluidic method. *Lab Chip.* 2014;15(2):557–562.
- [75] Angelova MI, Dimitrov DS. Liposome electroformation. *Faraday Discuss Chem Soc.* 1986;81:303–311.
- [76] Chen KL, Bothun GD. Nanoparticles meet cell membranes: probing nonspecific interactions using model membranes. *Environ Sci Technol.* 2014;48(2):873–880.
- [77] Hou W-C, Moghadam BY, Corredor C, et al. Distribution of functionalized gold nanoparticles between water and lipid bilayers as model cell membranes. *Environ Sci Technol.* 2012;46(3):1869–1876.
- [78] Rascol E, Devoisselle J-M, Chopineau J. The relevance of membrane models to understand nanoparticles–cell membrane interactions. *Nanoscale.* 2016;8(9):4780–4798.
- [79] Mayer LD, Hope MJ, Cullis PR. Vesicles of variable sizes produced by a rapid extrusion procedure. *Biochim Biophys Acta BBA – Biomembr.* 1986;858(1):161–168.
- [80] Needham D, McIntosh TJ, Evans E. Thermomechanical and transition properties of dimyristoylphosphatidylcholine/cholesterol bilayers. *Biochemistry (Mosc).* 1988;27(13):4668–4673.
- [81] MicroCal PEAQ-DSC automated – differential scanning calorimeter. Available from: <https://www.malvern.com/en/support/product-support/microcal-range/microcal-dsc-range/microcal-peaq-dsc-automated/>
- [82] Lindman S, Lynch I, Thulin E, et al. Systematic investigation of the thermodynamics of HSA adsorption to N-iso-Propylacrylamide/N-tert-Butylacrylamide copolymer nanoparticles. Effects of particle size and hydrophobicity. *Nano Lett.* 2007;7(4):914–920.
- [83] Cedervall T, Lynch I, Lindman S, et al. Understanding the nanoparticle–protein corona using methods to quantify exchange rates and affinities of proteins for nanoparticles. *Proc Natl Acad Sci.* 2007;104(7):2050–2055.
- [84] Joshi H, Shirude PS, Bansal V, et al. Isothermal titration calorimetry studies on the binding of amino acids to gold nanoparticles. *J Phys Chem B.* 2004;108(31):11535–11540.
- [85] Loosli F, Vitorazi L, Berret J-F, et al. Isothermal titration calorimetry as a powerful tool to quantify and better understand agglomeration mechanisms during interaction processes between TiO<sub>2</sub> nanoparticles and humic acids. *Env Sci Nano.* 2015;2(5):541–550.
- [86] Kettiger H, Québatte G, Perrone B, et al. Interactions between silica nanoparticles and phospholipid membranes. *Biochim Biophys Acta BBA – Biomembr.* 2016;1858(9):2163–2170.
- [87] Heerklotz H. The microcalorimetry of lipid membranes. *J Phys Condens Matter.* 2004;16(15):R441–R467.
- [88] Alig ARG, Gourdon D, Israelachvili J. Properties of confined and sheared Rhodamine B films studied by SFA–FECO spectroscopy. *J Phys Chem B.* 2007;111(1):95–106.
- [89] Anderson TH, Min Y, Weirich KL, et al. Formation of supported bilayers on silica substrates. *Langmuir.* 2009;25(12):6997–7005.

- [90] Israelachvili JN. Intermolecular and surface forces. London: Academic Press; 1992.
- [91] Burgess I, Li M, Horswell SL, et al. Influence of the electric field on a bio-mimetic film supported on a gold electrode. *Colloids Surf B Biointerfaces*. 2005;40(3–4):117–122.
- [92] Lipkowski J. Building biomimetic membrane at a gold electrode surface. *Phys Chem Chem Phys*. 2010;12(42):13874–13887.
- [93] Vakurov A, Galluzzi M, Podestà A, et al. Direct characterization of fluid lipid assemblies on mercury in electric fields. *ACS Nano*. 2014;8(4):3242–3250.
- [94] Schulz M, Olubummo A, Binder WH. Beyond the lipid-bilayer: interaction of polymers and nanoparticles with membranes. *Soft Matter*. 2012;8(18):4849–4864.
- [95] Moghadam BY, Hou W-C, Corredor C, et al. Role of nanoparticle surface functionality in the disruption of model cell membranes. *Langmuir*. 2012;28(47):16318–16326.
- [96] Richter R, Mukhopadhyay A, Brisson A. Pathways of lipid vesicle deposition on solid surfaces: a combined QCM-D and AFM study. *Biophys J*. 2003;85(5):3035–3047.
- [97] Shapero K, Fenaroli F, Lynch I, et al. Time and space resolved uptake study of silica nanoparticles by human cells. *Mol Biosyst*. 2011;7(2):371–378.
- [98] Nel A, Xia T, Meng H, et al. Nanomaterial toxicity testing in the 21st century: use of a predictive toxicological approach and high-throughput screening. *Acc Chem Res*. 2013;46(3):607–621.
- [99] Le Bihan O, Bonnafous P, Marak L, et al. Cryo-electron tomography of nanoparticle transmigration into liposome. *J Struct Biol*. 2009;168(3):419–425.
- [100] Michel R, Kesselman E, Plostica T, et al. Internalization of silica nanoparticles into fluid liposomes: formation of interesting hybrid colloids. *Angew Chem Int Ed*. 2014;53(46):12441–12445.
- [101] Roiter Y, Ornatka M, Rammohan AR, et al. Interaction of nanoparticles with lipid membrane. *Nano Lett*. 2008;8(3):941–944.
- [102] Zhang S, Nelson A, Beales PA. Freezing or Wrapping: the role of particle size in the mechanism of nanoparticle–biomembrane interaction. *Langmuir*. 2012;28(35):12831–12837.
- [103] Strobl FG, Seitz F, Westerhausen C, et al. Intake of silica nanoparticles by giant lipid vesicles: influence of particle size and thermodynamic membrane state. *Beilstein J Nanotechnol*. 2014;5(1):2468–2478.
- [104] Schneemilch M, , Quirke N. Submitted, 2017.